Journal of Nuclear Materials 384 (2009) 119–129

Contents lists available at ScienceDirect

Journal of Nuclear Materials

journal homepage: www.elsevier.com/locate/jnucmat

# Tungstate-based glass–ceramics for the immobilization of radio cesium

Elizabeth Drabarek, Terry I. McLeod, John V. Hanna, Christopher S. Griffith, Vittorio Luca *

*Australian Nuclear Science and Technology Organisation, Institute of Materials Engineering, New Illawarra Road, PMB 1, Menai, Lucas Heights, NSW 2234, Australia*

ARTICLE INFO

*Article history:*
Received 4 March 2008
Accepted 9 November 2008

ABSTRACT

The preparation of tungstate-containing glass–ceramic composites (GCC) for the potential immobilization of radio cesium has been considered. The GCC materials were prepared by blending two oxide precursor compositions in various proportions. These included a preformed Cs-containing hexagonal tungsten bronze (HTB) phase ($Cs_{0.3}Ti_{0.2}W_{0.8}O_3$, $P6_3/mcm$) and a blend of silica and other oxides. The use of the HTB phase was motivated on the assumption that a HTB-based adsorbent could be used to remove cesium directly from aqueous high level liquid waste feeds. In the absence of the HTB, glass–ceramics were relatively easily prepared from the Cs-containing glass-forming oxide blend. On melting the mixture a relative complex GCC phase assemblage formed. The principal components of this phase assemblage were determined using X-ray powder diffraction, $^{133}Cs$ MAS-NMR, and cross-sectional SEM and included glass, various zeolites, scheelite ($CaWO_4$) and a range of other oxide phases and Cs-containing aluminosilicate. Importantly, under no circumstance was cesium partitioned into the glass phase irrespective of whether or not the composition included the preformed Cs-containing HTB compound. For compositions containing the HTB, cesium was partitioned into one of four major phases including zeolite; Cs–silica–tungstate bronze, pollucite ($CsAlSi_2O_6$), and an aluminosilicate with an Al/Si ratio close to one. The leach resistance of all materials was evaluated and related to the cesium distribution within the GCC phase assemblages. In general, the GCCs prepared from the HTB had superior durability compared with materials not containing tungsten. Indeed the compositions in many cases had leach resistances comparable to the best ceramics or glass materials.



## 1. Introduction

There is an increasing awareness world wide that the adoption of advanced nuclear fuel recycling schemes as opposed to a once through cycle, or limited recycling, can have many important benefits such as enhanced fuel utilization and more efficient repository use. It is now well acknowledged and supported by extensive calculations that removal of between 99 and 99.9% of the U, Pu, Am and Cs and Sr can significantly reduce repository heat load and hence increase capacity by up to a factor of 50 [1–5]. In other words, the selective removal of high heat load elements from waste or used fuel can result in greatly enhanced repository utilization.

In cases where limited reprocessing has already occurred to remove U and Pu, or in waste liquids resulting from medical isotope production, it can also be desirable to remove the small quantities radio cesium and strontium remaining in the bulk using selective adsorbents or ion exchange materials. This can result in significant cost savings by permitting the disposal of the treated bulk liquid as low level waste grout [6,7]. Such volume and/or heat load reduction strategies have been the subject of a significant research effort resulting in the introduction of several new separations materials and methods [8–16].

Even though this strategy of concentrating activity onto a small volume of an adsorbent material allows the bulk of the waste to be disposed of much more easily, the disposal of the smaller volume of spent adsorbent still needs to be considered. Some possible disposal strategies include conversion of the materials to: (1) a tailored ceramic prepared from the adsorbent itself [17,18]; (2) glass made using either classical oxide precursors [19,20] or sol–gel precursors [21–24]; (3) conventional synroc-type ceramic material [25,26]; (4) a phosphate-based glass or ceramic [27]; (5) a glass–ceramic composite (GCC) material [28–30] or (6) a cementitious material [31,32].

In the case of highly Cs and Sr-selective titanosilicate adsorbents developed for the pre-treatment of HLW, it has been shown that glass formulations could be adapted to accommodate this spent adsorbent [33]. In addition, later studies have suggested that direct thermal conversion of the saturated adsorbents also represents an elegant (cradle-to-grave) approach to immobilization [18]. Similar cradle-to-grave strategies have been sought for other adsorbent materials including zeolites such as ferri-annite [34].

We have similarly shown recently that hexagonal tungsten bronze (HTB) based ion exchange materials can also be considered for the selective removal of both $^{137}Cs^+$ and $^{90}Sr^{2+}$ from acidic

* Corresponding author. Tel.: +61 2 9717 3087; fax: +61 2 9543 7179.
*E-mail address:* vlu@ansto.gov.au (V. Luca).

0022-3115/$ - see front matter Crown Copyright © 2008 Published by Elsevier B.V. All rights reserved.
doi:10.1016/j.jnucmat.2008.11.018

solutions [35–37]. It has also been demonstrated for these materials that it is viable to prepare a durable tailored ceramic directly from Cs- and Sr-saturated hexagonal tungsten bronze (HTB) selective adsorbent compounds with general formula $A_xWO_3$ or $A_xM_yW_{1-y}O_3$ where A cations can be Cs or Sr while M is an element that can substitute for W in the hexagonal tungsten bronze framework [38–41]. Given the potential of GCCs however, it is also of interest to explore the possibility of incorporating the saturated tungstate adsorbents into glass–ceramic composites. In this communication, we report results of investigations on the formation of glass–ceramic composites formed by combining calcined Cs-loaded hexagonal tungsten bronze materials with nominal composition $Cs_{0.3}Ti_{0.2}WO_3$ and a mixture of other oxide components. The composition of the latter oxide mixture was chosen to be similar to the alumina calcines generated by Idaho National Laboratory and investigated by Miller et al. [42] and from which cesium removal has been demonstrated using the composite ammonium molybdophosphate–polyacrylonitrile adsorbent. In the present experiments however, we also added $SiO_2$ to the oxide mixture in order to facilitate glass formation.

## 2. Experimental

### 2.1. Sample preparation

The GCC materials were prepared by combining 2.5 g of a preformed $Cs_{0.3}Ti_{0.2}W_{0.8}O_3$ HTB powder with glass forming oxides in various ratios as listed in Table 1. These materials were labelled **GCC-*x*** with *x* referring to the composition listed in this table. More specifically the glass forming oxide formulation essentially encompassed the addition of a certain proportion of silica to a composition resembling that of Idaho calcines [42]. The HTB starting material was prepared by blending $CsNO_3$ (Aldrich) with $TiO_2$ and tungstic acid $H_2WO_4$ (Aldrich) followed by heating to 1000 °C in air [41]. The $TiO_2$ was prepared through the hydrolysis of titanium (IV) isopropoxide (Aldrich) by the addition of water followed by washing and drying. The water content of this hydrous titanate material was determined by thermal analysis and compensated for during the blending with glass forming oxides.

After blending of the HTB precursor with the glass forming oxides the powder was transferred to a 40 mL platinum crucible and heated in a furnace in air according to two basic thermal protocols. The crucible was not covered. In protocol 1, the temperature was taken first to 1250 °C for 2 h and then 1300 °C for a further 2 h. The ramp rate was 10 °C/min and the cooling rate was 20 °C/min. Protocol 2 was similar to protocol 1 except that a single heating was carried out at 1300 °C for 2 h. Materials produced using protocol 2 and the compositions of Table 1 have been labelled **GCC-*x*a** as opposed to those of protocol 1 which were labelled **GCC-*x***.

### 2.2. Characterization

X-ray powder diffraction (XRD) patterns were recorded on a Scintag X1 diffractometer employing Cu Kα-radiation and a Peltier detector. The X-ray powder diffraction data were refined using the Rietveld program Rietica [43]. The background for each pattern was fitted by selecting points and fitting a cubic spline function through the selected points.

Secondary and backscattered electron images were obtained on a Jeol JSM6400 scanning electron microscope (SEM) operating at 15 keV. Samples were prepared by encasing in resin and cutting and polishing the surface to a roughness of less than 1 μm. Energy dispersive spectroscopy (EDS) analysis of the various phases observed in the cross-sections were obtained with a Noran Voyager (Noran) EDS system. Surface area measurements were performed on a Micromeritics ASAP 2010 instrument.

The elemental ratios in the GCC materials were determined by X-ray fluorescence (XRF) analysis using a wavelength dispersive Philips PW2400 X-ray fluorescence spectrometer equipped with a rhodium anode tube. Samples were prepared by pressing in boric acid. The program used for the quantification of the data was uniquant.

Solid-state high resolution $^{133}Cs$ magic-angle-spinning nuclear magnetic resonance (MAS-NMR) studies were undertaken at ambient temperatures on a Bruker MSL-400 (9.4 T) spectrometer operating at a $^{133}Cs$ frequency of 52.5 MHz. All 9.4 T data were acquired using a Bruker 4 mm MAS probe at frequencies of 15 kHz. The $^{133}Cs$ pulse conditions were calibrated on a 1 M CsCl solution from which a 'non-selective' π/2 pulse time of 6 μs was measured, which corresponds to a 'selective' π/2 pulse time for the spin-7/2 $^{133}Cs$ nucleus of 2 μs. From this calibration, a π/4 pulse time of 1 μs and a recycle delay of 3 s were implemented for all measurements. This 1 M CsCl solution was also used as a chemical shift reference thus representing $\delta = 0.0$ ppm.

### 2.3. Leaching

Because of the small specimen size of the individual melt samples prepared in this study, leach testing was carried out on irregular monoliths weighing between 0.1 and 0.4 g and having variable surface area. Leaching was conducted in de-ionized water at 90 °C for periods ranging from 1 to 14 days using a leach testing protocol based on ASTM C 1220 [44]. The major difference being the use of

**Table 1**
Target compositions for a range of GCC phase assemblages.

| | Targeted glass–ceramic compositions (wt% oxide) | | | | | | |
|---|---|---|---|---|---|---|---|
| | **1** | **2** | **3** | **4** | **5** | **6** | **7** |
| $Al_2O_3$ | 23.02 | 21.77 | 20.52 | 20.52 | 33.79 | 30.29 | 25.95 |
| $SiO_2$ | 11.10 | 19.43 | 27.76 | 27.76 | 8.77 | 14.61 | 21.92 |
| $CaF_2$ | 11.62 | 9.44 | 7.27 | 7.27 | 18.37 | 15.29 | 11.48 |
| $Na_2O$ | 4.00 | 3.49 | 2.98 | 2.98 | 6.12 | 5.27 | 4.21 |
| CaO | 8.98 | 12.34 | 15.69 | 15.69 | 9.95 | 11.82 | 14.17 |
| $Fe_2O_3$ | 0.39 | 0.32 | 0.24 | 0.24 | 0.61 | 0.51 | 0.38 |
| $Nd_2O_3$ | 0.31 | 0.25 | 0.19 | 0.19 | 0.49 | 0.41 | 0.30 |
| $Cs_2O$ | 7.05 | 5.73 | 4.41 | 4.41 | 21.19 | 21.16 | 21.12 |
| MgO | 0.38 | 0.31 | 0.24 | 0.24 | 0.59 | 0.00 | 0.37 |
| $Ti_2O$ | 2.62 | 2.13 | 1.64 | 1.64 | 0.00 | 0.00 | 0.00 |
| $WO_3$ | 30.44 | 24.73 | 19.03 | 19.03 | 0.00 | 0.00 | 0.00 |
| Total | 99.92 | 99.93 | 99.95 | 99.95 | 99.88 | 99.85 | 99.91 |
| gCs/g oxide | 0.0665 | 0.0540 | 0.0415 | 0.0415 | 0.1998 | 0.199 | 0.199 |

irregular monoliths rather than pieces with regular geometries. This was necessary because the small scale of the preparations made it difficult to cut from the melted mass such a piece of material. Also for this reason the discussion of leaching is framed mostly in terms of fractional Cs loss as an initial indicator of the inherent leachability of the GCC materials. Where normalized losses are quoted the specific surface area of the monoliths as measured by nitrogen porosimetry was used. These normalized losses (NL) were determined according to

$$\mathrm{NL} = \frac{C \cdot V}{F \cdot A} \quad (1)$$

where $C$ is the concentration of Cs released to solution; $V$, volume of solution; $F$, mass of Cs per g of sample, $A$, BET surface area.

The fractional Cs release, or elemental loss, $f$ is defined as $f = (W_0 - W_t)/W_0$ where $W_0$ is the initial Cs content in the solid phase and $W_t$ is the Cs content remaining in the solid phase after time $t$. Unless otherwise stated fractional elemental releases from powder materials were determined by loading the monoliths into 45 mL teflon jars to which was added 20 mL of demineralized water. The sealed jars were heated in a fan-forced oven in which the temperature was controlled to ±1 °C. The cooled acidic supernatant solutions were filtered through a 0.2 μm filter and analysed by inductively coupled plasma-mass spectrometry (ICP-MS).

## 3. Results

### 3.1. Characterization of tungsten bronze precursor phase

The GCC materials of interest in this work were prepared by heating together two main components. The first component was the preformed Cs-containing hexagonal tungsten bronze (HTB) precursor phase ($Cs_{0.3}Ti_{0.2}W_{0.8}O_3$, $P6_3/mcm$) prepared by calcination of mixtures of $CsNO_3$, $TiO_2$ and $H_2WO_4$ as described previously [41]. The second component was a mixture of $SiO_2$ and other components corresponding roughly to the published composition of Idaho calcines as explained in the introduction. Prior to characterizing the GCC phase assemblage resulting from the melting process it is first worth first considering the characterization and spectroscopic signature of Cs in the $Cs_{0.3}Ti_{0.2}W_{0.8}O_3$ HTB precursor material.

Fig. 1 shows the Rietveld refinement of the HTB precursor compound with nominal bulk composition, $Cs_{0.3}Ti_{0.2}W_{0.8}O_3$, used for the preparation of the glass–ceramics. It is apparent that as far as could be determined by XRD this material appeared ostensibly monophasic. Cross-sectional SEM (Fig. 2) on the other hand revealed in this sample two phases with similar electron contrast but different morphologies. The phase with fibrous morphology (phase 1) generally contained little if any M element (in this case

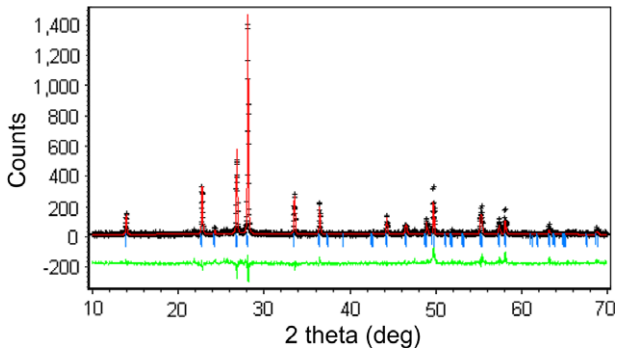


**Fig. 1.** Rietveld refinement of the $Cs_{0.3}Ti_{0.2}W_{0.8}O_3$ phase assemblage in space group $P6_3/mcm$.

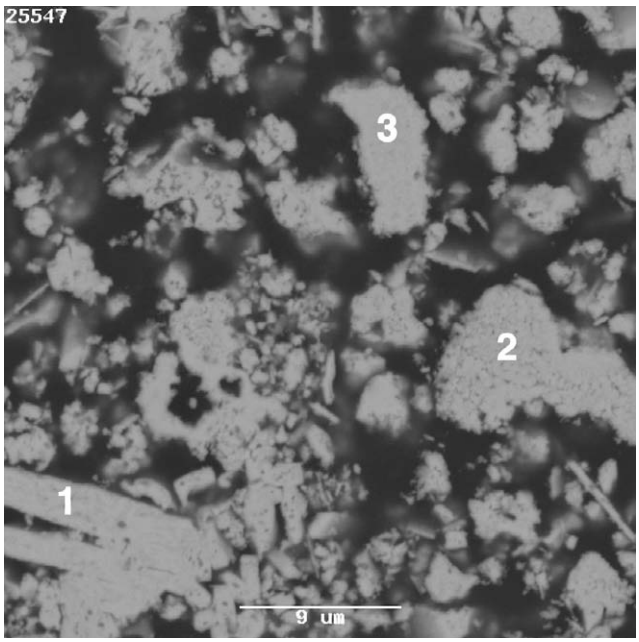


**Fig. 2.** Cross-sectional SEM image of the $Cs_{0.3}Ti_{0.2}W_{0.8}O_3$ precursor phase. Spot EDS analyses were: **1**, $Cs_{0.33}WO_3$; **2,** $Cs_{0.27}Ti_{0.13}W_{0.87}O_3$; and **3,** $Cs_{0.26}Ti_{0.20}W_{0.80}O_3$.

Ti) and high Cs content, while phases containing higher concentrations of M (e.g. phase 2 and 3 in Fig. 2), had slightly lower Cs contents consistent with previous observation for $Cs_xM_yW_{1-y}O_3$ bronze compounds [41].

The $^{133}$Cs MAS-NMR technique constituted a vital characterization technique in the identification of the Cs-bearing phases in the HTB assemblages assuming nominal compositions of $Cs_{0.3}M_{0.2}W_{0.8}O_3$, where M = Ti, Nb, Zr and Ta. From the $^{133}$Cs MAS-NMR data of Fig. 3, it is observed that two or more partially resolved resonances were always detected upon decomposition of these data, irrespective of the identity of the M cation.

For Ti- and Nb-containing phases (see Fig. 3(a) and (b)) only two unresolved resonances were observed; the $^{133}$Cs resonances at lower field were within −1 to −15 ppm range while the accompanying resonances at higher field were located within −35 to −50 ppm range. For Zr- and Ta-containing HTB phases more complex spectra were observed although the resonances again seemed to be grouped into two regions. Since the $Cs_{0.3}Ti_{0.2}W_{0.8}O_3$ progenitor phase of interest here exhibited precise chemical shifts of −12 and −50 ppm (see Table 3) from the lineshape decomposition of the spectrum in Fig. 3(a), these resonances can be confidently assigned to the Cs-rich and Cs-depleted HTB phases identified as comprising the $Cs_{0.3}Ti_{0.2}W_{0.8}O_3$ preparation, as discussed above.

### 3.2. Characterization of tungsten-containing GCCs – protocol 1

Having established the $^{133}$Cs MAS-NMR signature of the $Cs_{0.3}Ti_{0.2}WO_3$ precursor and related compounds, target compositions were prepared by mixing the $Cs_{0.3}Ti_{0.2}WO_3$ HTB composition and glass precursor oxide components so as to achieve the final compositions given in columns 1 to 4 of Table 1. In addition to these samples, compositions 5 to 7 were also prepared entirely from the oxide precursors with no tungsten included. That is, no HTB phases were included in these compositions in order to test the influence of tungstate and titanium. The actual chemical compositions of the GCCs produced by melting the compositions of Table 1 using protocol 1 (1250 °C/2 h + 1300 °C/2 h) are shown in Table 2. Note that while the compositions produced here contained between 10 and 20 wt% $CaF_2$, it was not possible to detect the

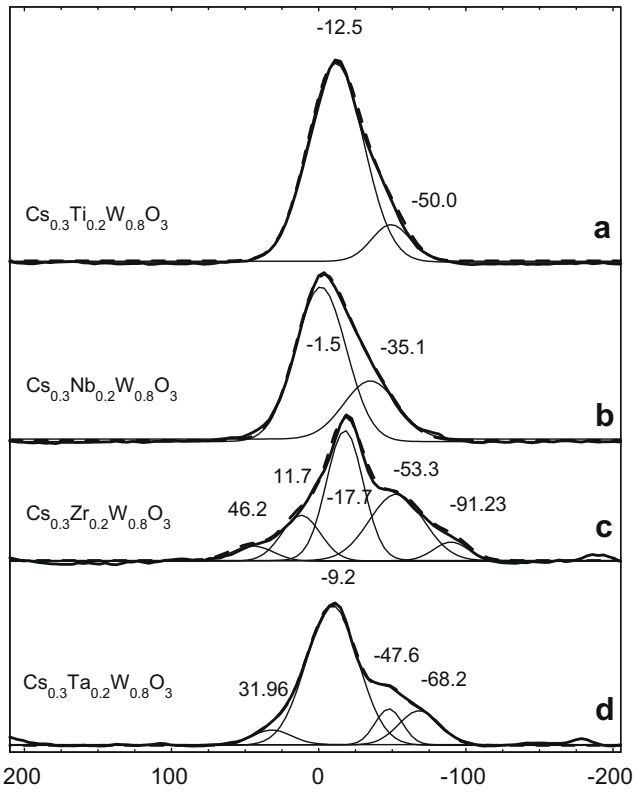


**Fig. 3.** Experimental $^{133}Cs$ MAS-NMR spectra of $Cs_{0.3}M_{0.2}W_{0.8}O_3$ phases with different substituent elements M: (a) Ti; (b) Nb; (c) Zr; and (d) Ta. Spectra decompositions are included.

fluorine using the energy dispersive X-ray analysis system applied here. The data of Table 2 shows that the experimentally determined $SiO_2$ and $Al_2O_3$ contents agreed well with the target values. The fact that these and other non-volatile elements were 'well behaved' attests to the accuracy of the analytical results. On the other hand the content of volatile elements such as Cs varied significantly from the target values. For instance, for the **GCC-1** composition with the lowest Si and highest W content (Al:Si:W of 1:0.5:1.3) the experimentally determined cesium content was only 0.34 wt% $Cs_2O$ instead of the 7 wt% targeted. The Cs analyses for the related mixtures, **GCC-2** and **-4** were also lower than the target values but not to the same degree as **GCC-1**. **GCC-5–7** without tungsten on the other hand showed variable Cs contents that ranged as much as 50% from the target values. However, even for **GCC-6** with similar Al/Si ratio to **GCC-1** much less Cs was volatilized. This might suggest that the particularly high Cs loss in the **GCC-1** composition was associated with the proportion of tungsten in the precursor blend. It is not unexpected that the volatilization of Cs would be high for the formation of the glasses and glass–ceramics prepared here at the temperatures used considering the small scale of the preparations. In the context of the present study however, we were not overly concerned with these volatilization losses and no special precautions were taken for their mitigation.

The XRD patterns of the **GCC-1–4** phase assemblages are shown in Fig. 4. These patterns provide an indication of the more abundant phases within the phase assemblage that is generated from compositions **1** to **4**. The XRD pattern of sample **GCC-1**, with the smallest silica content, showed evidence of a small amount of scheelite $CaWO_4$ (PCPDF 41-1431), although the pattern was dominated by reflections matching very well those of $WO_4^{2-}$-containing sodalite ($Na_6Ca_2(AlSiO_4)_6(WO_4)_2$, PDF 44-310). The formation of such $WO_4^{2-}$-containing sodalites was recently described by Lau et al. [45] as being possible by heating a mixture of zeolite-X and $WO_3$ to about 600 °C in air.

Reflections at 16.55° and 30.59° $2\theta$ in the pattern of **GCC-1** could be consistent with the presence of mullite but the visibility of only two reflections consistent with this phase makes its identification rather equivocal. The XRD patterns of **GCC-2** and **-3** were very similar to that of **GCC-1** indicating that the principal phases of the phase assemblages were sodalite and scheelite. In the pattern of the **GCC-4** phase assemblage it was possible to tentatively identify the reflections of the zeolite pollucite $CsAlSi_2O_6$ (PCPDF 29-407).

Back scattered electron images of **GCC-1** (Fig. 5) confirmed the existence of highly crystalline sodalite (phase 1) with Al/Si ratio close to 2 as the principal phase, which supports the XRD results. Plentiful quantities of scheelite ($CaWO_4$) were easily discerned as the phase with bright contrast (phase 2). There were also indications of small amounts of Ca- and Ti-rich intergrowths with Ca:Ti ratio of one (phases 3 and 4) which are likely to be a $CaTiO_3$ perovskite although the concentrations were too low to be detected by XRD.

Closer examination of **GCC-1** revealed the presence of a bright phase (phase 5) in the secondary electron image (Fig. 6(a)) that was difficult to detect in the back scattered electron image (Fig. 6(b)). The composition of this phase was found to be $Cs_{0.033}Na_{0.062}Ca_{0.210}Al_{0.240}Si_{0.336}Ti_{0.006}W_{0.114}$. In this phase the Al/Si ratio was close to 0.71 and was quite different to the large sodalite crystals in dark contrast analysing as $Na_{0.09}Ca_{0.31}Al_{0.26}Si_{0.12}$-$Ti_{0.14}W_{0.08}$ with Al/Si ~ 2 ratio. On the basis of the alkali and alkaline earth cation content, and the fact that the phase contained tungsten, it is suggested that this Cs-containing phase in **GCC-1** could be a different zeolite-like phase, which will be designated

**Table 2**
Chemical compositions of GCC phase assemblages after application of heating protocol 1 measured using XRF.

| | Found glass–ceramic compositions (wt% oxide) | | | | | | |
|---|---|---|---|---|---|---|---|
| | **1** | **2** | **3** | **4*** | **5** | **6** | **7** |
| $Al_2O_3$ | 25.11 | 23.23 | 21.78 | 21.39 | 41.31 | 38.01 | 28.11 |
| $SiO_2$ | 13.27 | 19.2 | 27.58 | 27.4 | 11.28 | 20.07 | 24.89 |
| $Na_2O$ | 5.59 | 4.19 | 3.56 | 3.29 | 6.32 | 5.91 | 4.42 |
| CaO | 20.72 | 21.01 | 23.51 | 23.26 | 29.18 | 29.3 | 25.61 |
| $Fe_2O_3$ | 0.52 | 0.414 | 0.31 | 0.34 | 0.89 | 0.687 | 0.494 |
| $Nd_2O_3$ | 0.19 | 0.213 | 0.181 | 0.182 | 0.615 | 0.494 | 0.332 |
| $Cs_2O$ | 0.34 | 3.81 | 3.06 | 4.15 | 8.77 | 3.9 | 14.88 |
| MgO | 0.41 | 0.32 | 0.24 | 0.237 | 0.73 | 1 | 0.54 |
| $Ti_2O$ | 1.84 | 1.74 | 1.4 | 1.43 | 0.02 | 0.02 | 0.018 |
| $WO_3$ | 30.23 | 24.38 | 17.32 | 17.24 | 0.53 | 0.023 | 0.031 |
| Total | 98.22 | 98.51 | 98.94 | 98.92 | 99.65 | 99.41 | 99.33 |
| gCs/g oxide | 0.0032 | 0.0359 | 0.0289 | 0.0391 | 0.0827 | 0.0368 | 0.1404 |

* As per protocol 1 only maximum temperature was 1250 °C.

**Table 3**
$^{133}$Cs MAS-NMR spectral decomposition results.

| Sample | Phase | $\delta$ (ppm) | FWHM (ppm) | Area (%) |
|---|---|---|---|---|
| HTB[a] | B | −12.0 | 44.4 | 88.8 |
| | B | −49.3 | 30.4 | 11.2 |
| **GCC-1** | P′ | 98.6 | 21.1 | 5.3 |
| | S | 2.5 | 64.9 | 94.7 |
| **GCC-2** | B | −25.9 | 104.1 | 28.8 |
| | B | −30.4 | 45.9 | 55.4 |
| | B | −50.5 | 18.7 | 15.7 |
| **GCC-3** | P | −6.4 | 40.7 | 93.7 |
| | B | −59.4 | 35.7 | 6.3 |
| **GCC-4** | P | −6.4 | 38.7 | 90.7 |
| | B | −49.0 | 19.4 | 9.3 |
| **GCC-1a** | P′ | 99.7 | 23.4 | 4.7 |
| | P | −7.8 | 54.2 | 86.0 |
| | Z | −54.4 | 10.1 | 9.2 |
| **GCC-2a** | P′ | 95.4 | 20.0 | 3.7 |
| | P | −15.2 | 44.1 | 60.2 |
| | Z | −54.6 | 13.5 | 36.1 |
| **GCC-3a** | P | −4.5 | 38.6 | 94.2 |
| | Z | −49.5 | 17.7 | 5.8 |
| **GCC-5** | P′ | 97.0 | 12.4 | 28.4 |
| | ? | −22.4 | 106.4 | 71.6 |
| **GCC-6** | P | −11.7 | 40.8 | 74.9 |
| | Z | −53.7 | 13.9 | 25.1 |
| **GCC-7** | P′ | 97.4 | 7.9 | 65.4 |
| | P | −17.8 | 50.7 | 21.5 |
| | Z | −46.9 | 26.2 | 13.1 |

B, bronzoid; P, pollucite; P′, $CsAlSiO_4$ with nepheline structure; S, sodalite; Z, high Al sodalite.
[a] $Cs_{0.3}Ti_{0.2}W_{0.8}O_3$.

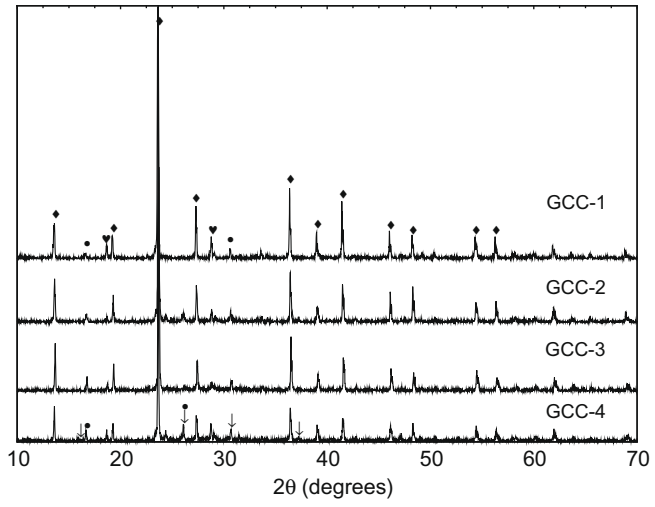


**Fig. 4.** XRD patterns of glass–ceramics of varying composition. Assignments of various reflections are: ♦, sodalite; ↓, pollucite; ♥, scheelite; and ■, mullite.

Z. It proved impossible to locate any pollucite in this sample indicating that, if this phase was present, its abundance must be very low. This is consistent with our assessment of the XRD data.

For **GCC-2** with a higher overall Cs content (Table 2), and for which XRD also showed the principal phase to be sodalite, the phase assemblage had a similar qualitative appearance to **GCC-1**. Unlike **GCC-1** however, detailed cross-sectional SEM examination (Fig. 7) revealed that the major crystalline sodalite phase (phase 1 with Al/Si ~ 2) in this instance contained neither Cs nor W. Amorphous regions of very dark contrast with composition – $Ca_{0.44}Al_{0.10}Si_{0.35}Ti_{0.06}$ (phase 3) were consistent with glass while minor amounts of $CaTiO_3$ perovskite (phase 4) were also apparent. The vast majority of the Cs in **GCC-2** was however, concentrated in very large amorphous regions of bright contrast (phase 5) with

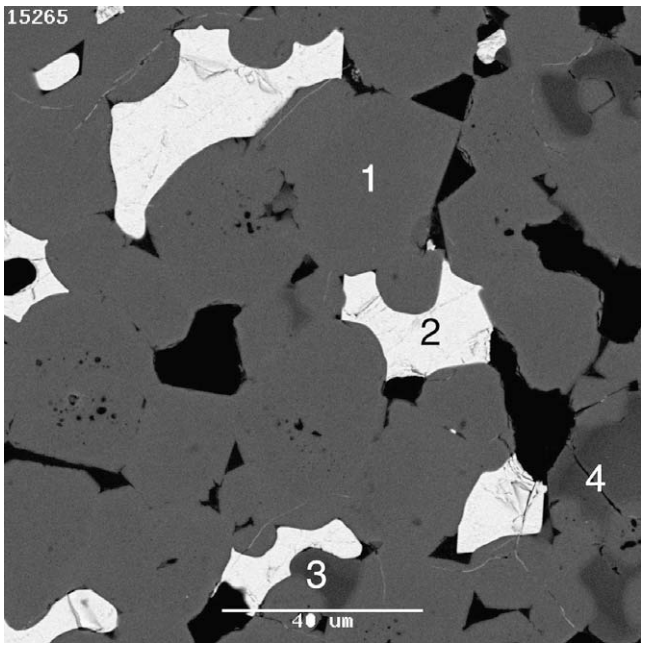


**Fig. 5.** Back-scattered electron image of the cross-section of **GCC-1**: **1**, $Na_{0.09}Ca_{0.31}Al_{0.26}Si_{0.12}Ti_{0.14}W_{0.08}$ (sodalite); **2**, $Ca_{0.5}W_{0.5}$ (scheelite); **3**, $Ca_{0.49}Ti_{0.46}$ (perovskite); and **4**, $Ca_{0.49}Ti_{0.46}$.

composition $Cs_{0.198}Na_{0.031}Si_{0.522}W_{0.244}$. In addition, very small quantities of a Cs-containing aluminosilicate with Al/Si ~ 0.5 (phase 2) were able to be located. The Al/Si ratio of phase 2 and the high Cs content suggests that this is pollucite. Exhaustive SEM investigations failed to locate Cs anywhere else in this sample.

The cross-sectional SEM of **GCC-3** and **-4** were similar to **GCC-2** and are shown in Fig. 8. These samples were prepared from the same initial composition but **GCC-4** was melted at slightly lower temperature. Both images showed an abundance of glass in very dark contrast (phase 1) and zeolite in lighter contrast (phase 2) having about the same Si/Al ratio of about 0.5. Pollucite (phase 3, Si/Al ~ 2) was easily located in both samples and was the only Cs-containing phase that could be identified.

Cs-133 MAS-NMR spectra of **GCC-1** to **-4** are shown in Fig. 9. For **GCC-1** the major species exhibited a resonance at $\delta = 2.5$ ppm although an additional low intensity resonance at $\delta = 99$ ppm was also present. According to Ashbrook et al. [46] the latter resonance is indicative of $CsAlSiO_4$ with Si/Al = 1. While the existence of this phase with Al/Si ~ 1 which will henceforth be designated P′ was unequivocal by NMR, its abundance was clearly low as judged by decomposition of the spectral envelope (Table 3). Such a low abundance would understandably account for the difficulty in locating this phase by SEM. On the other hand, it was possible to locate by SEM a Cs-containing zeolite-like phase in the **GCC-1** sample with composition $Cs_{0.033}Na_{0.062}Ca_{0.210}Al_{0.240}Si_{0.336}Ti_{0.006}W_{0.114}$ (Si/Al ~ 1.4). The dominant 2.7 ppm chemical shift (95% of the total spectrum) for the **GCC-1** sample must therefore be associated with this phase which was identified by SEM. Indeed Mon et al. [47] in their study of Cs-containing zeolites showed that a resonance with approximately similar line width to that observed here and having a similar shift (−2.3 ppm c.f. 2.7 ppm) was attributable to Cs in the β cages of sodalite. A broad line width and extensive spinning side band pattern was indicative of a motionally restrictive environment as compared with LTA (Linde Type A) zeolites which give a single, narrow, motionally average line. Therefore, given the similarity in chemical shift and line width we assign the 2.7 ppm resonance observed in the spectrum of **GCC-1** to Cs in sodalite (S) (also called $\beta$) cages.

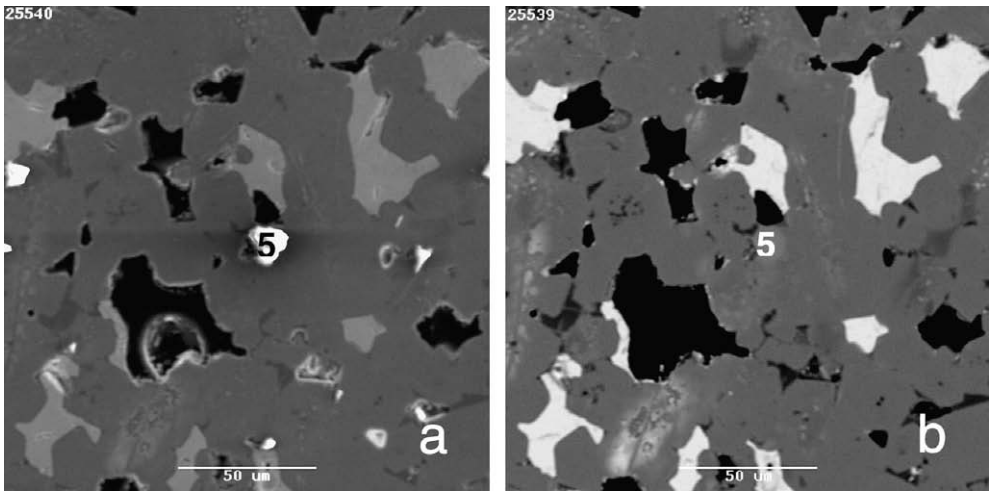


**Fig. 6.** (a) Secondary and (b) back scattered electron image of Cs-containing phase in **GCC-1**. Analysis of phase 5 is $Cs_{0.033}Na_{0.062}Ca_{0.210}Al_{0.24}Si_{0.336}Ti_{0.006}W_{0.114}$.

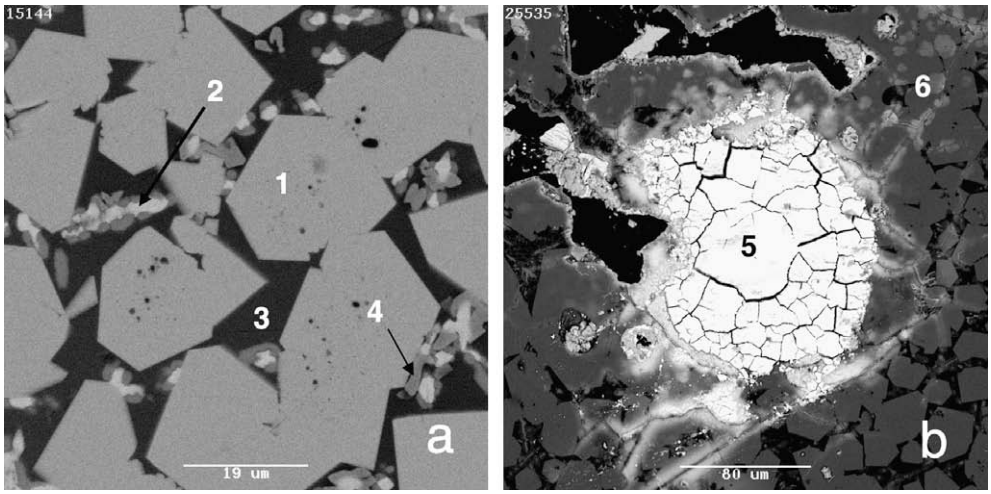


**Fig. 7.** Back scattered electron images of **GCC-2**: **1**, $Na_{0.10}Ca_{0.26}Al_{0.36}Si_{0.15}$ (zeolite); **2**, $Cs_{0.20}Al_{0.25}Si_{0.4}$ (pollucite); **3**, $Ca_{0.44}Al_{0.10}Si_{0.35}Ti_{0.06}$ (glass); **4**, $Ca_{0.39}Ti_{0.49}$ (perovskite), **5**, $Cs_{0.198}Na_{0.031}Al_{0.003}Si_{0.522}Ti_{0.003}W_{0.244}$ (bronzoid); and **6**, $Na_{0.061}Ca_{0.206}Al_{0.225}Si_{0.373}W_{0.105}$.

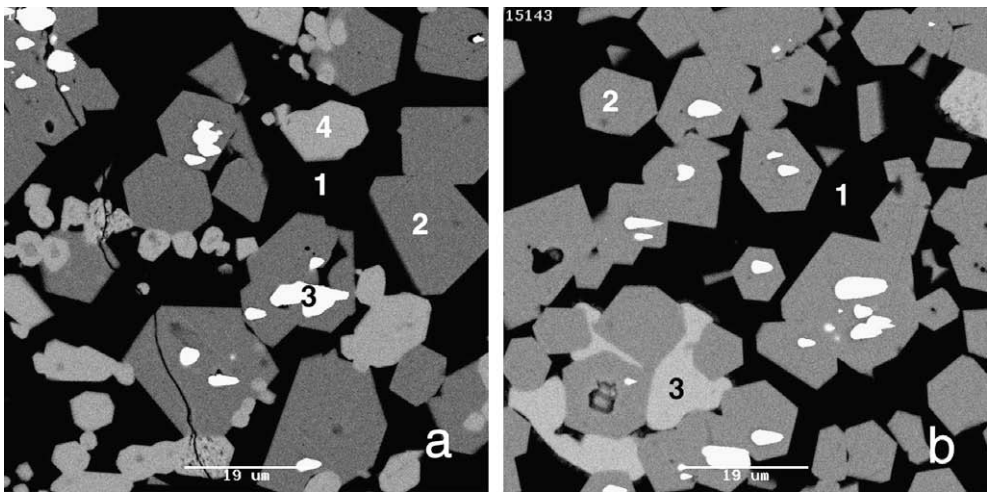


**Fig. 8.** Back scattered electron images of: (a) **GCC-3**: **1**, $Na_{0.02}Ca_{0.37}Al_{0.16}Si_{0.41}Ti_{0.035}$ (glass); **2**, $Na_{0.10}Ca_{0.26}Al_{0.35}Si_{0.15}$ (sodalite); **3**, $Ca_{0.52}W_{0.45}$ (scheelite); **4**, $Cs_{0.18}Al_{0.25}Si_{0.50}$ (pollucite). (b) **GCC-4**: **1**, $Na_{0.03}Ca_{0.36}Al_{0.19}Si_{0.39}Ti_{0.03}$ (glass); **2**, $Na_{0.10}Ca_{0.26}Al_{0.33}Si_{0.18}$ (sodalite); and **3**, $Cs_{0.23}Al_{0.25}Si_{0.52}$ (pollucite).

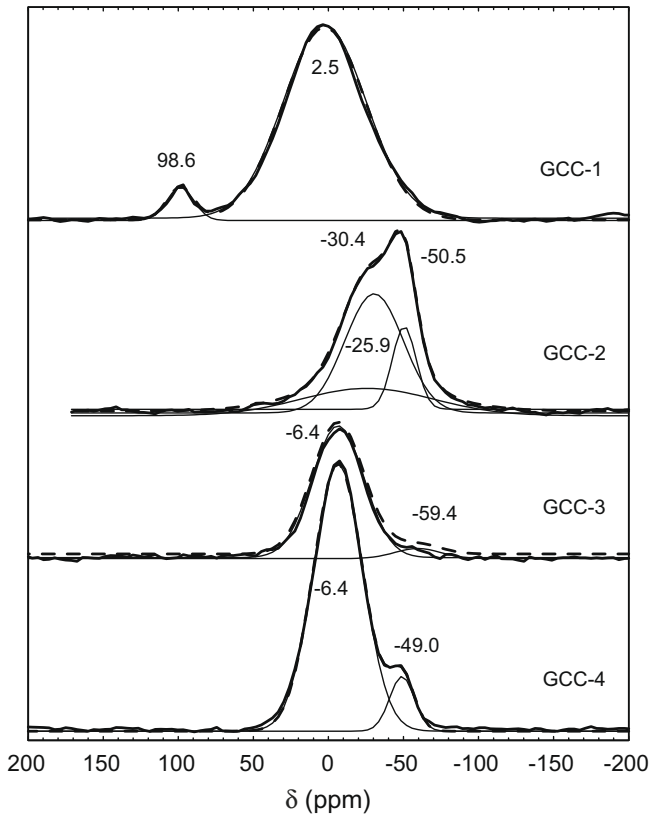


**Fig. 9.** $^{133}$Cs MAS-NMR of glass–ceramic composites made from $Cs_{0.3}M_{0.2}W_{0.8}O_3$ phases and glass formers. Samples **GCC-1** to **GCC-3** were produced by heating to 1250 °C for 2 h followed by 1300 °C for 2 h.

The $^{133}$Cs MAS-NMR of **GCC-2** consisted of two relatively narrow chemical shifts at −30.4 and −50.5 ppm. It was not possible to discount the existence of an additional very broad feature centered at −25.9 ppm. These relatively sharp resonances had similar linewidths and were at similar chemical shifts to what was observed in the series of $Cs_{0.3}Ti_{0.2}W_{0.8}O_3$ compound (Fig. 1). The major Cs-containing phase observed in the **GCC-2** sample by SEM was that with composition $Cs_{0.198}Si_{0.522}W_{0.244}$ and we therefore assign the NMR shifts at −26 and −47 ppm to Cs in such Si-containing HTB phases. For **GCC-3** and **-4** the $^{133}$Cs MAS-NMR spectra were dominated by a shift at about −6.4 ppm accounting for greater than 90% of the total area (Table 3). This is clearly consistent with assignment to pollucite (P) as per the observations of Ashbrook et al. [46] and is in accord with the SEM results discussed previously. At least in the XRD pattern of the **GCC-4** phase assemblage it was possible to unequivocally confirm the existence of this mineral phase. The identity of the phases responsible for the minor resonances at about −50 ppm in the spectra of **GCC-3** and **-4** is unclear but based solely on the $^{133}$Cs chemical shift, this suggests that poorly crystalline, Cs-containing bronzed phases may also present in these phase assemblages.

### 3.3. Characterization of tungsten-containing GCCs – protocol 2

To examine the effect of, or tolerance to, variations in heating protocol for the HTB-glass compositions we carried out an identical set of experiments as for **GCC-1–4** only using protocol 2 which involved a single temperature excursion to 1300 °C for 2 h. In general, phase analysis of these samples (labelled **GCC-1a** through **-3a**) revealed phase assemblages which were broadly similar to those of the samples heated for longer times (**GCC-1–3**) with some notable differences. As an example we show in Fig. 10(a) the cross-sectional SEM of the **GCC-2a** composition. As in the **GCC-1–4** series it was possible in **GCC-2a** to readily identify four phases including, glass, sodalite (S), pollucite (P) and the Cs-containing 1:1 aluminosilicate phase referred to as P′. It proved to be a relatively straight forward exercise to locate cesium in the latter two phases (P and P′) while no cesium could be found in the glass phase even after exhaustive inspection. However, some very fine grained phases were observed in localized regions (Fig. 10(b), region 5). The fine grained nature of the material precluded analysis of the individual particles, however, analysis of a cluster of grains proved possible and returned compositions such as $Cs_{0.058}Ca_{0.332}Na_{0.019}Al_{0.434}Si_{0.15}W_{0.033}$ and $Cs_{0.037}Ca_{0.18}Na_{0.019}Al_{0.49}Si_{0.226}W_{0.046}$. The Al/Si in this fine grained material was in general somewhat greater than two and the presence of a large amount of Ca and some Na suggests that this is likely to be a zeolitic phase (Z).

The $^{133}$Cs MAS-NMR spectra for the GCCs phase assemblages prepared using protocol 2 (**GCC-1a–3a**) are shown in Fig. 11. In general for all of these samples it was possible to confirm location of cesium in three phases. Like the samples prepared using heating protocol 1 (1250 °C/2 h then 1300 °C/2 h) most of the cesium was located in pollucite phases ($\delta = -8$ ppm) which accounted for 86%, 60% and 94% of the Cs containing phases in the spectra of

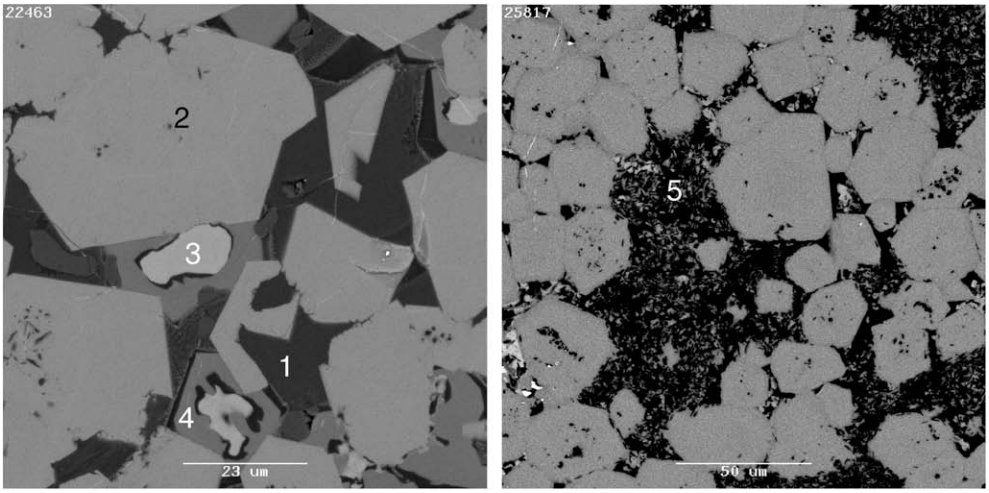


**Fig. 10.** Back-scattered electron image of the cross-section of **GCC-2a**: **1**, $Cs_{0.004}Na_{0.036}Ca_{0.295}Al_{0.217}Si_{0.341}Ti_{0.098}W0.007$ (glass); **2**, $Na_{0.10}Ca_{0.27}Al_{0.365}Si_{0.134}W_{0.13}$ (sodalite); **3**, $Cs_{0.246}Al_{0.24}Si_{0.468}$ (pollucite); **4**, $Cs_{0.126}Na_{0.013}Ca_{0.198}Al_{0.317}Si_{0.353}$ (P′); and **5**, $Cs_{0.058}Ca_{0.332}Na_{0.019}Al_{0.434}Si_{0.15}W_{0.033}$.

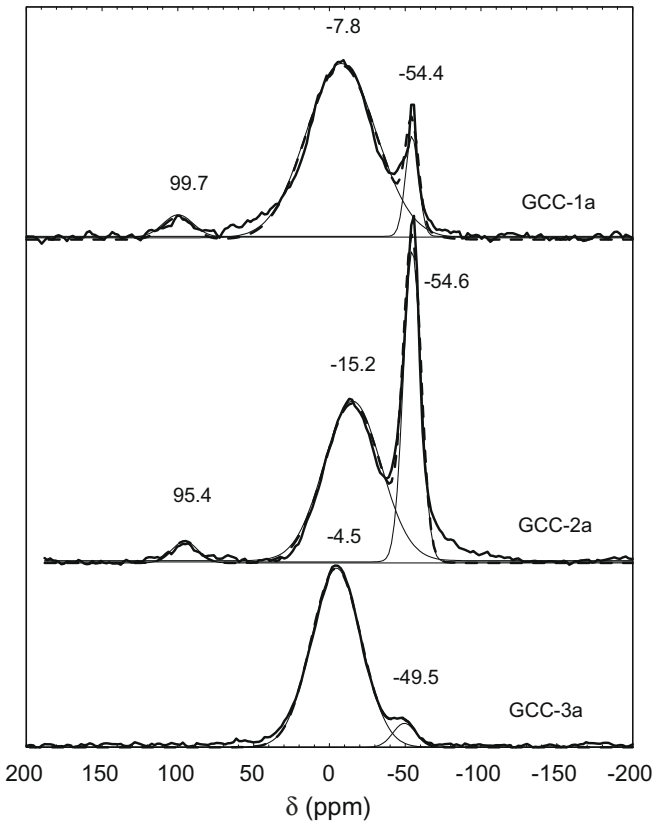


**Fig. 11.** $^{133}$Cs MAS-NMR of glass–ceramic composites made from $Cs_{0.3}Ti_{0.2}W_{0.8}O_3$ and glass formers. Samples **GCC-1a** to **-3a** were produced using protocol 2 which entailed heating to 1300 °C for 2 h.

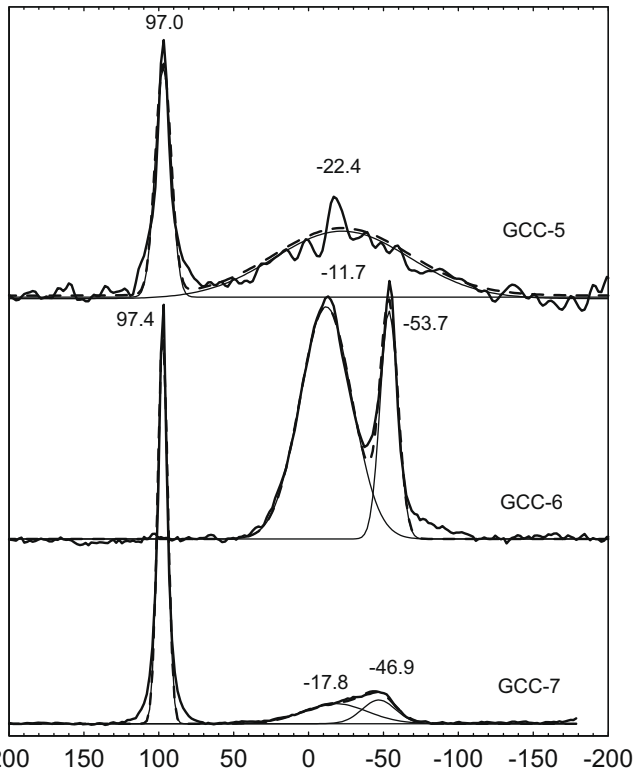


**Fig. 12.** $^{133}$Cs MAS-NMR of glass–ceramic composites made from $CsNO_3$ and glass formers. (a) **GCC-5**; (b) **GCC-6**; and (c) **GCC-7**. No tungsten was included in these compositions.

**GCC-1a**, **-2a** and **-3a**, respectively, as determined by decomposition of the spectra (Table 2). The spectra of samples **GCC-1a** and **-2a** showed, in addition, evidence for the presence of the 1:1 aluminosilicate P′ phase ($\delta = 99$ ppm) and a sharp resonance at $\delta = -52$ ppm which constituted a significant proportion of the spectrum. Given that the SEM analyses showed the clear existence of a third Cs-containing aluminosilicate in each phase assemblage which was probably a zeolitic phase with Al/Si ~ 2, it follows that the −52 ppm resonance should be assigned to this phase (Z′) which accounts for about 36% of the spectrum of **GCC-2a** (see Table 3). Indeed, as previously mentioned, cesium in zeolitic cages can give rise to such sharp resonances.

### 3.4. Characterization of GCCs without tungsten

For comparison purposes it was of interest to determine how the phase distribution of the glass–ceramics would be influenced by the absence of tungsten. To this end samples were prepared from mixtures of $CsNO_3$ and glass formers (see **GCC-5** to **-7** in Table 2) followed by heating to 1300 °C for 2 h.

Having shown that $^{133}$Cs MAS-NMR is easily able to discriminate Cs in different phases in these samples, it is clear from the MAS-NMR data of Fig. 12 that all of these tungsten-free samples contained cesium in each of the three previously identified Cs-containing phases although the proportions varied according to the exact composition of the precursor powders. Clearly the Cs-containing 1:1 aluminosilicate phase P′ was present in abundance in **GCC-5** and **-7**. However, this phase was barely perceptible in the **GCC-6** sample in which the dominant phase (75%) resonance was that at −11.7 ppm. Although the chemical shift of this resonance was somewhat larger than that of the previously observed pollucite, its linewidth was very much consistent with pollucite. The −53.7 ppm resonance observed in **GCC-6** had similar linewidth to the Z phase identified in the **GCC-1a–3a** series of samples. A small amount of both the P and Z phases would also appear to exist in **GCC-7**.

### 3.5. Leaching studies

The cumulative fractional Cs loss from **GCC-1–7** phase assemblages are plotted in Fig. 13 as a function of time. It is apparent that most of the Cs was leached from **GCC-1** in a relatively short time. Such poor Cs retention indicates that the putative Cs-containing

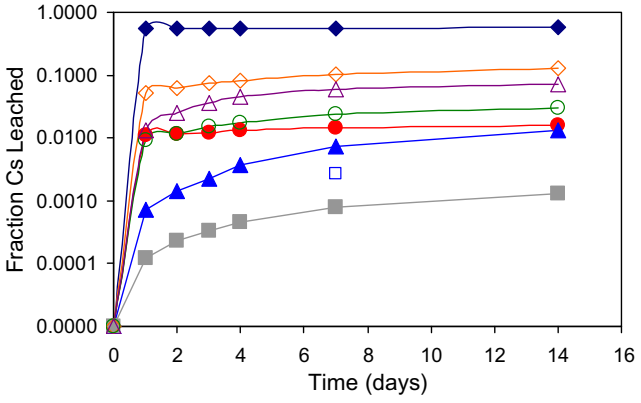


**Fig. 13.** Fraction of Cs leached as a function of time for compositions 1 to 7: ♦, **GCC-1**; ●, **GCC-2**; ▲, **GCC-3**; ■, **GCC-4**; ◇, **GCC-5**; ○, **GCC-6**; and △, **GCC-7**. The □ symbol represents the 7-day fractional loss for a sample of $Ba_{0.9}Cs_{0.3}Al_{2.1}Ti_{5.9}O_{16}$ hollandite prepared by hot uniaxial pressing.

sodalite phase S in which most of the Cs appears to reside in this sample is a poor Cs host matrix. In comparison, for **GCC-2** where the bulk of the Cs was located in the bronzoid phase (B), the cumulative fractional Cs loss was extremely low as it was for **GCC-3** and **-4** where greater than 90% of the Cs was located in pollucite. Generally speaking, when tungsten was not included in the compositions, such as for **GCC-5–7**, inferior performance was observed.

It is interesting to note that by far the best performance was observed for **GCC-4** (0.1% Cs leached after 14 days) where Cs was almost exclusively located in a pollucite (P) phase. This level of cesium retention is comparable with some Cs-loaded HTB and hollandite ceramics which give up about the same proportion of Cs after a similar period of time and under similar experimental conditions. With the exception of **GCC-1** where Cs appeared to be located principally in a sodalite phase (S), **GCC-2**, **-3** and **-4** had superior performance compared with samples prepared from compositions not containing tungsten.

The variation in Cs loss for the W-containing GCC compositions prepared using protocol 2 (**GCC-1a–3a**) are shown in Fig. 14. The variation in the order of leach resistance of this series of samples did not follow a similar order to the comparable compositions prepared using protocol 1. However, in general the best of these materials **GCC-1a** and **-3a** gave quite good performances. The poorest performance was obtained for the **GCC-2a** composition which previously returned a much better performance under protocol 1. The superior performance of **GCC-1a** and **-3a** agreed with the fact that a large proportion of Cs partitioned in the pollucite phase of these assemblages (see decomposition results in Table 3).

Due to the small sample size prepared of each GCC composition, the resultant phase assemblages were relatively porous due to considerable air bubble incorporation. Therefore, in order to put the leach characteristics of the GCC samples on a comparative basis with those of other more conventional waste form materials we present in Table 4 the normalized losses (NL) of Cs in g solid/$m^2$/day as measured over a 7 days period. These data show that while **GCC-1** releases most of its cesium in a relatively short time period, the normalized loss over 7 days is actually very good at $1.65 \times 10^{-4}$ g solid/$m^2$/day. This value represents almost an order of magnitude better normalized Cs loss than any of the other GCC phase assemblages. This is due to the fact that the **GCC-1** monolith actually has quite a high specific surface area. The data of Table 4 also reveal several other features of the leach characteristics of the GCC materials. Firstly, in general the tungsten containing phase assemblages display superior performance (lower NL) as

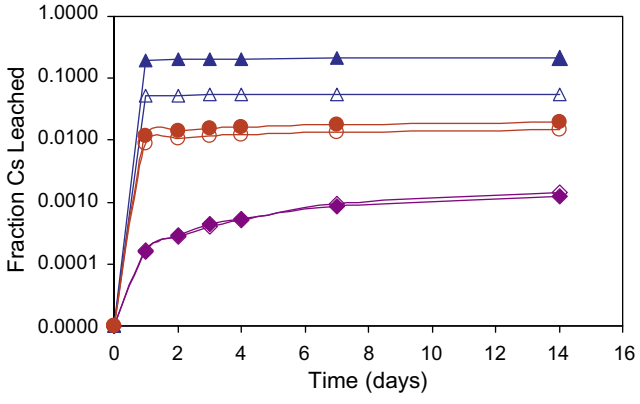


**Fig. 14.** Fraction of Cs leached as a function of time for compositions 5 to 7: ♦, **GCC-1a**; ◇, **GCC-2a**; ▲, **GCC-3a**; △, **GCC-1a′**; ●, **GCC-2a′**; and ○, **GCC-3a′**. The data designated with ′′ represent duplicate experiments.

**Table 4**
Normalized Cs losses (NL) after 7 days in g solid/$m^2$/day for various GCCs in comparison with other more conventional ceramic waste form materials. Cs-hol corresponds to reference Cs-hollandite phases prepared by hot uniaxial pressing (HUP) or sintering (SIN). S is the BET surface area.

| | S ($m^2$/g) | NL (g solid/$m^2$) |
|---|---|---|
| **GCC-1** | 0.118 | 4.76 |
| **GCC-2** | 0.0524 | 0.28 |
| **GCC-3** | 0.00273 | 2.15 |
| **GCC-4** | 0.0253 | 0.03 |
| **GCC-5** | 0.013 | 7.67 |
| **GCC-6** | 0.0114 | 1.35 |
| **GCC-7** | 0.181 | 0.33 |
| $Cs_{0.3}Ti_{0.2}W_{0.8}O_3$ | 0.255 | 0.12 |
| Cs-hol (HUP) | 0.0046 | 0.037 |
| Cs-hol (SIN) | 0.273 | 0.074 |

compared with those assemblages not containing tungsten but most importantly, the NLs are comparable with those of sintered (SIN) and hot uniaxially pressed (HUP) Cs-containing hollandites, and indeed the parent $Cs_{0.3}Ti_{0.2}W_{0.8}O_3$ bronze.

## 4. Discussion

Lambregts and Frank [28] characterized glass-bonded ceramic waste forms developed by Argonne National Laboratories which were designed for the immobilization of fission product and minor actinide-containing salt electrolyte derived from the pyroelectrometallurgical treatment of irradiated nuclear fuel assemblies from the EBR-II reactor. This glass-bonded ceramic waste form was generated by mixing salt-occluded LTA sodalite zeolite samples ($2Na_8(Al_6Si_6O_{24})Cl_{12}$) with borosilicate glass frits (66.5 wt% $SiO_2$, 19.1 wt% $B_2O_3$, 6.8 wt% $Al_2O_3$, 7.1 wt% $Na_2O$, 0.5 wt% $K_2O$) in a 3:1 ratio and heating in air to 915 °C. The occluded zeolites were generated by heating the appropriate salts and zeolites in a mixer at 550 °C. These glass-bonded ceramics had Al/Si ratios that were close to one and so are spanned by the compositions investigated in that study. Additionally, between 17% and 47% of the Cs initially occluded in the zeolitic phase was found in the resultant glass phase for compositions containing 100%, 50% and 25% occluded Cs. *Importantly, none of the cesium initially occluded in the zeolite remained in the zeolite.* Some was instead found to reside in a pollucite phase which formed at the boundary between the glass and the other zeolites, with the remainder partitioning into the glass. Subsequently, Ebert et al. have conducted a detailed inter-laboratory product consistency test (PCT) comparison of the durability of these glass-bonded waste forms [48]. This has clearly demonstrated that Al, Na and Si are easily leached from such waste forms under modest conditions. Morss et al. have also reported the results of leaching tests on glass-bonded sodalite waste forms including for Ce, Nd and U [49,50]. Again relatively poor results were obtained for these elements also. Simpson and colleagues [51] have provided a detailed description of the processing of glass-bonded sodalite and also provided PCT leaching test results that include Cs. Indeed, they have reported normalized Cs and Sr losses of 0.109 and 0.067 g/$m^2$, respectively, for a 7-day PCT that are relatively poor compared with other ceramics. In studies in which the salt-occluded zeolite was not heated Lewis et al. [52] have reported leach results at least one order of magnitude better than borosilicate glass.

In the present study, in which higher temperatures have been employed, abundant concentrations of Cs-containing glass and sodalite might have been expected to form on the basis of the studies outlined above. Using the unique localized perspective provide by $^{133}Cs$ MAS-NMR we have instead found that significant sodalite phase formation was only observed where the Al/Si ratio

was highest ie. **GCC-1** and -**2**, and in the case of **GCC-1** almost exclusively as a $WO_4^{2-}$ sodalite. Interestingly, cesium did not partition into the glass phase in either of these two cases.

For the **GCC-1** composition (Al:Si:W of 1:0.5:1.3) in which a significant proportion of the initially included cesium was volatilized, the remaining cesium based on the results of the $^{133}$Cs MAS-NMR data appeared to partition exclusively into two phases. The majority of the cesium (95%) in the **GCC-1** composition partitioned into a phase with composition $Cs_{0.033}Na_{0.062}Ca_{0.210}Al_{0.24}Si_{0.336}Ti_{0.006}W_{0.114}$. Based on the high alkali and alkaline metal content, the fact that tungsten was present, and the $^{133}$Cs chemical shift, we believe this phase is most probably sodalite or a sodalite-like phase (labelled S in Table 3). Only 5% of this cesium partitioned into what we have termed the P′ phase (Table 3) with approximate composition $CsAlSiO_4$ as identified by Ashbrook et al. [46]. Examination of the data of Fig. 13 and Table 4 shows that of the tungsten containing phases this composition had particularly poor leach characteristics.

According to Vasil'eva et al. [53] and their studies with coal fly ash, the compositionally similar $NaAlSiO_4$ phase, dominates when M:Al:Si is close to 1:1:1 (M being an alkali metal). This phase can crystallize in both the hexagonal (nepheline) and cubic (carnegieite) space groups, and hence, we propose that the P′ phase is likely to be one of these structure types. Although the $CsAlSiO_4$ phase (P′) was also identified in the **GCC-1a** and **-2a** phase assemblages produced using protocol 2, the relative percentage of Cs which partitioned into these phases was small (<5% total) so little can be said regarding its leach resistance. The P′ phase was also a major component of the **GCC-5** composition which returned poor performance in terms of both fractional (Fig. 13) and normalized Cs loss (Table 4). In contrast Vasil'eva et al. [53] have shown that the leaching of Al, Si, K, and Ca from natural framework aluminosilicate, in structures with equal or close ratios between the silicon, aluminum, and alkali metal contents (nepheline and sodalite with the ratio Na:Al:Si = 1:1:1 or 1.33:1:1), occurs at comparable rates that are considerably lower than those from borosilicate and aluminophosphate glasses. Furthermore, studies on nepheline/glass phases by Bulbulian et al. have shown that excellent leach resistance is exhibited by such phase assemblages formed directly from $Co^{2+}$ loaded zeolite A ($Na_{12}Si_{12}Al_{12}O_{48}\cdot xH_2O$) and X ($Na_{86}Si_{106}Al_{86}O_{384}\cdot xH_2O$) [54].

Of the tungsten containing compositions, the particularly poor leach characteristics exhibited by the **GCC-1** assemblage can therefore be rationalized in terms of the percentage of Cs which resides in the tungstate–sodalite phase S and to a lesser extent the P′ phase. Mitigation against the formation of this poorly leach resistant sodalite phase in our approach appears possible by increasing the relative proportion of silica and reducing that of tungsten. Moreover, an additional effect of these changes is that Cs volatilization is reduced and that the partitioning behavior of cesium is significantly (but systematically) altered. It should be reiterated that we have not attempted in this study to address volatilization (of Cs) issues although the apparent ability to reduce this potential problem through simple addition of silica is encouraging. It is also important to stress that the present study is carried out at very small scale which would exacerbate such volatilization losses compared to larger scale preparations.

For **GCC-2** (Al:Si:W = 1:0.9:1.14) the bulk of the cesium partitioned into the bronzoid phase (B) which, based on previous studies, and the present results, is quite durable. At still higher silica contents (Al:Si:W = 1:1.35:0.93) and still lower tungsten contents (**GCC-3 and -4**), pollucite (P) with Al/Si ~ 0.5 dominated the Cs-containing phase assemblage with only about 5–10% in another zeolite-like phase (Z) being responsible for the relatively narrow chemical shifts at about −50 ppm. This suggests total incorporation of Cs into either the B or P phases and exclusion of Cs from the glass confer excellent durability comparing favorably with reference waste form materials such as hollandites prepared by hot uniaxial pressing (HUP) or sintering (SIN). From the **GCC-2a** composition produced using protocol 2 and for which a resonance at comparable chemical shift accounted for 36% of the spectrum it was possible to observe compositions such as $Cs_{0.037}Ca_{0.18}Na_{0.019}Al_{0.49}Si_{0.226}W_{0.046}$ with Al/Si close to 2. Such an Al/Si ratio is not consistent with sodalite having the usual Al/Si ratio of one and certainly the chemical shift is far removed from that normally associated with Cs in the $\beta$ cages of such sodalites (~−2.6 ppm) [47]. On the other hand, it should be noted that sodalites can have variable Al/Si ratios and indeed even pure aluminate sodalites of the general composition $M_8(AlO_2)_{12}X_2$ are known where M is a divalent cation, e.g. Ca, Sr, and Cd, and X is a divalent anion, e.g. $SO_4^{2-}$, $CrO_4^{2-}$, $WO_4^{2-}$, $O^{2-}$, $S^{2-}$, Se, and Te [55]. To our knowledge, no $^{133}$Cs MAS-NMR has ever been reported for such high aluminum containing sodalites. Therefore, it is still possible that the Z phase represents a sodalite with high Al/Si ratio. The increased normalized Cs-loss for this phase is also highly suggestive that the Z phase is of the sodalite structure.

From a durability perspective many of the mineral phases identified here have well known durability. For example, GCC waste forms based on pollucite were first described from the early 1970s [56,57]. They are even the subject of patents [58]. Xu et al. [59] have examined the crystal chemistry and phase transitions in substituted pollucites along the $CsAlSi_2O_6$–$CsTiSi_2O_{6.5}$ join and have shown that compositions such as $CsTi_xAl_{1-x}Si_2O_{6+0.5x}$ for which $0 < x < 1$ are possible. Interestingly, even though we have Ti in the present oxide blend, Ti-containing pollucite does not appear to form. In this study, we have observed the partitioning of Cs into the channels of a range of zeolite-like structures including the bronze, sodalite and high Al sodalites but were not able to observe cesium in the glass phase. Apart from the phase assemblage rich in sodalite (**GCC-1**) leach resistance was good.

The reasons for complete partitioning of Cs away from the glass and into pollucite and other moderately durable phases in this study is intriguing. It is our assertion however, that the most probable reason for this is the high Ca content of our compositions. The Ca appears to partition preferentially into the glass phase which presumably saturates the glass with respect to non-glass forming alkali and alkaline earth cations. Moreover, this effect is no doubt aided by the fact that only low Cs contents have been explored. It must be stated however, that although exhaustive SEM–EDS analysis have been undertaken for each GCC phase assemblage, small quantities could reside in the glass phase that are below the detection limits of the EDS technique.

## 5. Conclusions

- Using low silica and high tungsten contents of the initial compositions (Al:Si:W of 1:0.5:1.3) resulted in quite high Cs volatilization losses. The remaining Cs was predominantly partitioned into a poorly durable sodalite phase.
- For compositions containing higher silica (Al:Si:W of 1:0.9:1.14) content the Cs was principally partitioned into a highly durable bronzed phase that was quite different to the initial HTB material used.
- At still higher silica contents (Al:Si:W of 1:1.35:0.93) partitioning of Cs into pollucite was favored. These compositions also gave highly durable materials.
- Tungsten present in the initial composition was essentially soaked up by the principal Cs-free sodalite phase and generally had a beneficial influence on the durability of the phase assemblages as compared to GCC products containing no tungsten.

## References


[1] R.A. Wigeland, T.H. Bauer, T.H. Fanning, E.E. Morris, Nucl. Technol. 154 (2006) 95.
[2] R.A. Wigeland, T.H. Bauer, R.N. Hill, J.A. Stillman, J. Nucl. Sci. Technol. 44 (2007) 415.
[3] T.A. Todd, R.A. Wigeland, Advanced Separation Technologies for Processing Spent Nuclear Fuel and the Potential Benefits to a Geologic Repository (Amer. Chemical Soc., 1155, Sixteenth st., NW, Washington DC 20036 USA), vol. 933, pp. 41–55.
[4] M. Ozawa, T. Suzuki, S.I. Koyama, H. Akatsuka, H. Mimura, Y. Fujii, Prog. Nucl. Energy 50 (2008) 476.
[5] C.W. Forsberg, Nucl. Technol. 131 (2000) 252.
[6] T.A. Todd, N.R. Mann, T.J. Tranter, F. Sebesta, J. John, A. Motl, J. Radioanal. Nucl. Chem. 254 (2002) 47.
[7] S.M. Robinson, F.J. Homan, ORNL/TM-13433 (1997). 13 pp.
[8] A. Dyer, M. Pillinger, J. Newton, R. Harjula, T. Moller, S. Amin, Chem. Mater. 12 (2000) 3798.
[9] T.A. Todd, K.N. Brewer, D.J. Wood, P.A. Tullock, N.R. Mann, L.G. Olson, Sep. Sci. Technol. 36 (2001) 999.
[10] D.T. Hobbs, M.J. Barnes, R.L. Pulmano, K.M. Marshall, T.B. Edwards, M.G. Bronikowski, S.D. Fink, Sep. Sci. Technol. 40 (2005) 3093.
[11] G.J. Lumetta, M.J. Wagner, E.O. Jones, Sep. Sci. Technol. 30 (1995) 1087.
[12] J. Rais, P. Selucky, N.V. Sistkova, J. Alexova, Sep. Sci. Technol. 34 (1999) 2865.
[13] M.A. Lilga, R.J. Orth, J.P.H. Sukamto, S.D. Rassat, J.D. Genders, R. Gopal, Sep. Purif. Technol. 24 (2001) 451.
[14] T. Moller, R. Harjula, A. Paajanen, Sep. Sci. Technol. 38 (2003) 2995.
[15] M.A. Norato, M.H. Beasley, S.G. Campbell, A.D. Coleman, M.W. Geeting, J.W. Guthrie, C.W. Kennell, R.A. Pierce, R.C. Ryberg, D.D. Walker, J.D. Law, T.A. Todd, Sep. Sci. Technol. 38 (2003) 2647.
[16] T. Tomasberger, A.C. Veltkamp, A.S. Booij, U.W. Scherer, Radiochim. Acta 89 (2001) 145.
[17] M. Nyman, T.M. Nenoff, Y. Su, M.L. Balmer, A. Navrotsky, H. Xu, Mater. Res. Soc. Symp. Proc. 556 (1999) 71.
[18] Y. Su, M.L. Balmer, L. Wang, B.C. Bunker, M. Nyman, T. Nenoff, A. Navrotsky, Mater. Res. Soc. Symp. Proc. 556 (1999) 77.
[19] D.E. Harrison, J.M. Pope, S. Wood, EP Patent 42770 (1981).
[20] M.J. Pope, D.E. Harrison, EP Patent 44149 (1982).
[21] A. Mathur, US Patent 5494863 (1996).
[22] L.H. Cadoff, D.B. Smith-Magowan, US Patent 04759879.
[23] E.J. Lahoda, EP Patent 205313 (1986).
[24] R.W. Chickering, B.E. Yoldas, B.H. Neuman, EP Patent 46085 (1982).
[25] A.E. Ringwood, S.E. Kesson, N.G. Ware, W. Hibberson, A. Major, Nature 278 (1979) 219.
[26] A.E. Ringwood, US Patent 4274976 (1981).
[27] M.G. Mesko, D.E. Day, J. Nucl. Mater. 273 (1999) 27.
[28] M.J. Lambregts, S.M. Frank, Microporous Mesoporous Mater. 64 (2003) 1.
[29] M.C. Hash, C. Pereira, M.A. Lewis, R.J. Blaskovitz, V.N. Zyryanov, J.P. Ackerman, Ceram. Trans. 72 (1996) 135.
[30] W.E. Lee, M.I. Ojovan, M.C. Stennett, N.C. Hyatt, Advance. Appl. Ceramics 105 (2006) 3.
[31] C.A. Langton, D. Singh, A.S. Wagh, M. Tlustochowicz, K. Dwyer, Ceram. Trans. 107 (2000) 175.
[32] M.L.D. Gougar, B.E. Scheetz, D.D. Siemer, Nucl. Technol. 125 (1999) 93.
[33] M.K. Andrews, P.J. Workman, Ceram. Trans. 93 (1999) 171.
[34] Z. Klika, Z. Weiss, M. Mellini, M. Drabek, Appl. Geochem. 21 (2006) 405.
[35] V. Luca, C.S. Griffith, H. Chronis, J. Widjaja, H. Li, N. Scales, Mat. Res. Soc. Symp. Proc. 807 (2004) 309.
[36] C.S. Griffith, V. Luca, Chem. Mater. 16 (2004) 4992.
[37] C.S. Griffith, V. Luca, P. Yee, F. Sebesta, Sep. Sci. Technol. 40 (2005) 1781.
[38] V. Luca, E. Drabarek, C.S. Griffith, H. Chronis, J. Foy, Mat. Res. Soc. Symp. Proc. 807 (2004) 303.
[39] C.S. Griffith, F. Sebesta, J.V. Hanna, P. Yee, E. Drabarek, M.E. Smith, V. Luca, J. Nucl. Mater. 358 (2006) 151.
[40] V. Luca, C.S. Griffith, E. Drabarek, H. Chronis, J. Nucl. Mater. 358 (2006) 139.
[41] V. Luca, E. Drabarek, H. Chronis, T. Mcleod, J. Nucl. Mater. 358 (2006) 164.
[42] C.J. Miller, A.L. Olson, C.K. Johnson, Sep. Sci. Technol. 32 (1997) 37.
[43] C.J. Howard, B.A. Hunter, A Computer Program for Rietveld Analysis of X-ray and Neutron Powder Diffraction Patterns, vol. 1, Lucas Heights Research Laboratories, NSW, Australia, 1998.
[44] ASTM C1220, Annual Book of ASTM Standards, V. 12.01.
[45] C. Lau, S. Bruck, H.J. Mai, U. Kynast, Microporous Mesoporous Mater. 47 (2001) 339.
[46] S.E. Ashbrook, K.R. Whittle, L. Le Polles, I. Farnan, J. Am. Ceram. Soc. 88 (2005) 1575.
[47] J. Mon, Y. Deng, M. Flury, J.B. Harsh, Microporous Mesoporous Mater. 86 (2005) 277.
[48] W.L. Ebert, M.A. Lewis, S.G. Johnson, J. Nucl. Mater. 305 (2002) 37.
[49] L.R. Morss, M.L. Stanley, C.D. Tatko, W.L. Ebert, Mat. Res. Soc. Symp. Proc. 608 (2000) 733.
[50] L.R. Morss et al., J. Alloys Compd. 303 (2000) 42.
[51] M.F. Simpson, K.M. Goff, S.G. Johnson, K.J. Bateman, T.J. Battisti, K.L. Toews, S.M. Frank, T.L. Moschetti, T.P. O'holleran, W. Sinkler, Nucl. Technol. 134 (2001) 263.
[52] M.A. Lewis, D.F. Fischer, L.J. Smith, J. Am. Ceram. Soc. 76 (1993) 11–2826.
[53] N.G. Vasil'eva, N.N. Anshits, O.M. Sharonova, M.V. Burdin, A.G. Anshits, Glass Phys. Chem. 31 (2005) 637.
[54] S. Bulbulian, P. Bosch, J. Nucl. Mater. 295 (2001) 64.
[55] S.E. Dann, P.J. Mead, M.T. Weller, Inorg. Chem. 35 (1996).
[56] A. De, B. Luckscheiter, W. Lutze, G. Malow, E. Schiewer, Atomwirtschaft, Atomtechnik 20 (1975) 359.
[57] G.H. Beall, H.L. Rittler, Adv. Ceram. 4 (1982) 301.
[58] R.M. Morena, US Patent 5094677.
[59] H.W. Xu et al., J. Am. Ceram. Soc. 85 (5) (2002) 1235.